Aerosol and Air Quality Research, 18: 2121–2130, 2018

ISSN: 1680-8584 print / 2071-1409 online
doi: 10.4209/aaqr.2018.02.0059

Enhanced Activity of Nb-modified CeO_2/TiO_2 Catalyst for the Selective Catalytic Reduction of NO with NH_3

Ye Jiang[1*], Changzhong Bao[1], Shaojun Liu[2], Guitao Liang[1], Mingyuan Lu[1], Chengzhen Lai[1], Weiyun Shi[1], Shiyuan Ma[1]

[1] *College of Pipeline and Civil Engineering, China University of Petroleum, Qingdao 266580, China*
[2] *State Key Laboratory of Clean Energy Utilization, Zhejiang University, Hangzhou 310027, China*

ABSTRACT

A series of CeO_2-Nb_2O_5/TiO_2 catalysts were prepared by an impregnation method and investigated for the selective catalytic reaction (SCR) of NO with NH_3. The 15 wt.% CeO_2–10 wt.% Nb_2O_5/TiO_2 catalyst (CeNbTi) exhibited the highest activity and resistance to a high gas hourly space velocity and K_2O. In the presence of H_2O and SO_2, it also showed better activity than the CeTi catalyst. The addition of Nb could improve the dispersion of CeO_2 and increase the amount of Ce^{3+} and chemisorbed oxygen species on the catalyst surface, which enhances the catalytic activity of CeTi. The superior SCR activity of CeNbTi might also be attributed to its high redox ability, the enhanced adsorption capacity of NH_3 species and the synergistic action between Ce, Nb and Ti species.

Keywords: Selective catalytic reduction; NO; NH_3; CeO_2-Nb_2O_5/TiO_2; Impregnation method.

INTRODUCTION

Selective catalytic reduction (SCR) of NO_x with NH_3 has been a dominant technique to remove NO_x in the exhaust gas from stationary and mobile sources (Nakajima and Hamada, 1996; Busca *et al.*, 1998; Du *et al.*, 2018). V_2O_5/TiO_2-based materials are widely adopted because of their high activity and good resistance to SO_2 (Busca *et al.*, 1998; Fu *et al.*, 2014). However, this type of materials is effective only within a narrow temperature range of 300–400°C. Quite a few unavoidable disadvantages still exist, such as the toxicity of vanadium, high conversion of SO_2 to SO_3 with increasing vanadium loadings (Dunn *et al.*, 1998) and low N_2 selectivity at high temperatures (Yates *et al.*, 1996). Consequently, there has been a great interest to modify current catalysts and investigate novel catalysts to substitute vanadium with other transition metals (Mn, Fe, Cu, etc.) (Li *et al.*, 2017) to overcome the above-mentioned disadvantages.

In recent years, tremendous attention has been paid to cerium-based oxides for the SCR of NO with NH_3, such as CeO_2/TiO_2 (Xu *et al.*, 2008; Gao *et al.*, 2010b; Shan *et al.*, 2011; Li *et al.*, 2012), CeO_2/Al_2O_3 (Shen *et al.*, 2009; Guo *et al.*, 2013), MnO_x-NbO_x-CeO_2 (Chen *et al.*, 2015), CeO_2-MoO_3/TiO_2 (Liu *et al.*, 2014; Jiang *et al.*, 2015a), CeO_2-WO_3/TiO_2 (Chen *et al.*, 2010; Shan *et al.*, 2012; Jiang *et al.*, 2015b; Zhao *et al.*, 2016) and NbO_x/CeO_2-ZrO_2 (Ma *et al.*, 2015). These compounds were found to have the ability to store and release oxygen via the redox shift between Ce^{4+} and Ce^{3+} under oxidizing and reducing conditions, respectively. Due to the acidic nature of Nb species, the introduction of Nb_2O_5 was correlated with the improvement in the NH_3-SCR activity and N_2 selectivity over VO_x/CeO_2 (Lian *et al.*, 2015), V_2O_5/TiO_2 (Vikulov *et al.*, 1994), MnO_x-CeO_2 (Casapu *et al.*, 2010) and MnO_x (Lian *et al.*, 2014). In addition, the tolerance to SO_2 or/and H_2O could be also enhanced over VO_x/CeO_2 catalyst (Lian *et al.*, 2015). These observations motivated us to add niobium oxide to Ce/Ti catalyst to adjust its physicochemical properties, so as to enhance its SCR activity.

METHODS

Catalyst Preparation

The CeO_2-Nb_2O_5/TiO_2 catalysts were prepared by an impregnation method. A desired amount of niobium oxalate ($C_{10}H_5NbO2_0$), cerium nitrate ($Ce(NO_3)_3{\cdot}6H2O$) and citric acid was dissolved into deionized water, in which the molar ratio of precursor salts/citric acid was 2:1. Next, the solution was mixed with TiO_2. After exposed to ultrasonic energy for 30 min, the mixture was continuously stirred and heated in water bath at 70°C. At last, the resulted solids were dried at 110°C overnight, followed by calcination at 500°C for 5 h in air. The catalysts were

* Corresponding author.
Tel.: +86-532-86981767; Fax: +86-532-86981882
E-mail address: jiangye@upc.edu.cn

denoted as Ce_xNb_yTi, where x and y represented the mass percentage of CeO_2 and Nb_2O_5 to TiO_2, respectively.

The K_2O-poisoned samples were prepared by impregnating Ce_xTi or Ce_xNb_yTi catalyst with aqueous solution of potassium nitrate. The mixture was evaporated to dryness at 70°C on a water bath, dried at 110°C overnight, and calcined at 500°C in air for 5 h. In this work, the molar ratio of K/Ce was set as 0.1.

Activity Measurement

The SCR activity tests of the catalysts were carried out in a fixed-bed quartz flow reactor (i.d. = 8 mm; L = 600 mm) using 0.19 g catalysts with 60–100 mesh in the temperature range of 150–500°C. The feed gas mixture contained 1000 ppm NO, 1000 ppm NH_3, 3 vol.% O_2, 10 vol.% H_2O (when used), 200 ppm SO_2 (when used) and N_2 as balance gas. Water vapor was generated through the injection of H_2O in a heated pipe. Under ambient conditions, the total flow rate was 500 mL min^{-1} and the gas hourly space velocity (GHSV) was 90,000 h^{-1}. The concentrations of NO, SO_2 and O_2 in the feed gas was tested by a gas analyzer (350 Pro, Testo). The concentrations of NO_2 and N_2O were recorded by an FT-IR gas analyzer (DX-4000, Gasmet).

Catalysts Characterization

The BET surface area of the catalyst samples was measured by N_2 adsorption/desorption analysis at 77 K with ASAP2020-M (Micromeritics Instrument Corp.). Prior to the surface area measurement, the sample was degassed in vacuum at 300°C for 4 h.

Powder X-ray diffraction (XRD) measurements were conducted on a X'Pert PRO diffractometer (Panalytical Corp.) with Cu Ka radiation at 40 kV and 40 mA.

X-ray photoelectron spectra (XPS) were recorded on a Thermo ESCALAB 250 spectrometer using Al Ka X-rays (hv = 1486.6 eV) as a radiation source at 150 W. Binding energies of Ce 3d and O 1s were calibrated using carbon deposit C 1s peak (BE = 284.8 eV).

Microstructures of the catalyst samples were observed with a JOEL JEM-2100F Electron Microscope.

The H_2 temperature programmed reduction (H_2-TPR) and NH_3 temperature programmed desorption (NH_3-TPD) were performed on FINESORB-3010 chemisorption analyzer (FINETEC Instruments Corp.) with 0.1 g of the catalysts with a thermal conductivity detector (TCD). TPR runs were carried out in a flow of H_2 (10%) in Ar (30 mL min^{-1}) from room temperature to 800°C, with a heating rate of 10°C min^{-1}. For NH_3-TPD, the sample was pretreated at 500°C in He for 1 h, then it was cooled down and exposed in a 0.5% NH_3/He (30 mL min^{-1}) gas flow for 1 h, followed by flushing with He for 1 h, the sample was then heated up to 700°C with a rate of 10°C min^{-1} in flowing He.

RESULTS AND DISCUSSION

NH_3-SCR Performance

Effect of CeO_2 and Nb_2O_5 Loadings

To find the optimal Ce loading, Nb_2O_5 loading was kept at 10 wt.% TiO_2 and the NO conversion as a function of temperature was compared over various catalysts under different GHSV in Fig. 1. At the GHSV of 90,000 h^{-1}, $Nb_{10}Ti$ exhibited negligible activity in the temperature range of 150–350°C. Afterward, its NO conversion increased with increasing reaction temperature and the maximum NO conversion (92.0%) was obtained at 500°C. After the addition of Ce, NO conversion increased sharply over $Nb_{10}Ti$. Higher Ce loading enhanced SCR activity and widened the temperature window until the mass percentage of CeO_2/TiO_2 reached 15. Further increasing Ce loading caused the slight decrease in SCR activity below 275°C. In a wide temperature range 250–450°C, 93.9–98.8% NO conversion was obtained at the GHSV of 90,000 h^{-1} over $Ce_{15}Nb_{10}Ti$. As shown in Fig. 1(b), when the GHSV reached 200,000 h^{-1}, the NO conversion was up to 92.1–99.4% over $Ce_{15}Nb_{10}Ti$ in the temperature range of 275–500°C. In contrast, the NO conversions of other samples dramatically

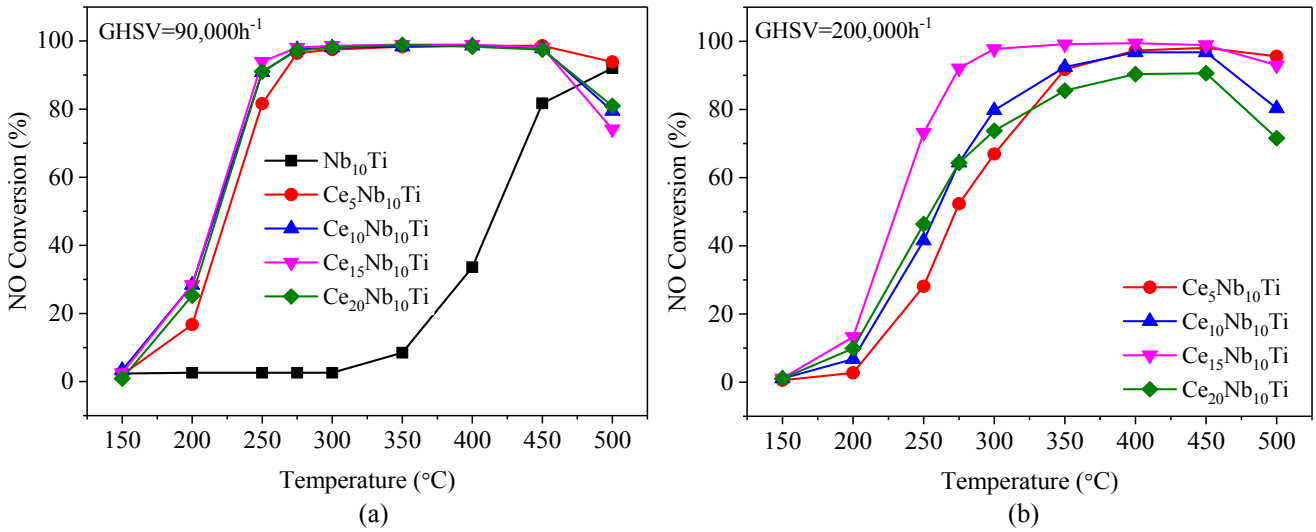

Fig. 1. NH_3-SCR activities over various catalysts with different CeO_2 loadings under different GHSV. Reaction conditions: [NO] = [NH_3] = 1000 ppm, [O_2] = 3 vol.%, balance N_2 and GHSV = (a) 90,000 h^{-1} and (b) 200,000 h^{-1}.

decreased at 250–400°C. These indicated that $Ce_{15}Nb_{10}Ti$ catalyst was highly effective for NO reduction at a high GHSV of 200,000 h^{-1}.

The effect of Nb_2O_5 loading on the NO conversion of Ce-Ti oxide at GHSV of 90,000 h^{-1} and 200,000 h^{-1} is exhibited in Fig. 2. As shown in Fig. 2(a), different Nb loadings led to the increase in the catalytic activity of $Ce_{15}Ti$ to different extents. When Nb_2O_5 loading was lower than 20%, the NO conversion was not nearly influenced by Nb_2O_5 loading and remained nearly 100% in the temperature range of 275–450°C. $Ce_{15}Nb_{10}Ti$ presented the best catalytic activity and the NO conversion reached up to 98.1% at about 275°C. Further increase in Nb loading resulted in a conspicuous decline in catalytic activity. When the GHSV was increased to 200,000 h^{-1}, except $Ce_{15}Nb_{10}Ti$, the NO conversions of the other samples dramatically decreased at 250–450°C. $Ce_{15}Nb_{10}Ti$ still maintained high catalytic activity (Fig. 2(b)).

Fig. 3 compares the N_2O concentration over $Ce_{15}Ti$ and $Ce_{15}Nb_{10}Ti$. The yield of N_2O increased with increasing reaction temperatures over the two samples. Their N_2O concentrations were very close below 300°C. When the reaction temperature was higher than 300°C, the introduction of Nb could inhibit the generation of N_2O distinctly. The N_2O concentration over $Ce_{15}Nb_{10}Ti$ was only about 10 ppm at 450°C. It indicated that Nb could improve the N_2 selectivity of $Ce_{15}Ti$ especially at high temperatures.

The Influence of K_2O

Fig. 4 displays the influence of K_2O on the catalytic activities of $Ce_{15}Ti$ and $Ce_{15}Nb_{10}Ti$. K_2O could inhibit the SCR activity of $Ce_{15}Ti$ remarkably and its NO conversion decreased from 95.9% to 43.4% at 350°C due to K_2O doping. Although the NO conversions also dropped over $Ce_{15}Nb_{10}Ti$ in the presence of K_2O, 89.3–98.0% NO conversion was still obtained at 275–450°C. It was clear that the addition of Nb could significantly enhance its resistance to K_2O of Ce-Ti oxide.

The Influence of H_2O and SO_2

The effect of H_2O on the SCR activities of $Ce_{15}Ti$ and $Ce_{15}Nb_{10}Ti$ was investigated and the results are shown in Fig. 5. The presence of H_2O led to the decrease in the NO conversions over both samples. However, $Ce_{15}Nb_{10}Ti$ exhibited higher SCR activities than $Ce_{15}Ti$. In the temperature range of 350–450°C, the NO conversion of $Ce_{15}Nb_{10}Ti$ decreased slightly and still maintained about 90%. It should be noted that H_2O had a positive impact on the activities of both catalysts at 500°C. The similar phenomena were observed over other Ce-Ti oxide catalysts (Gao *et al.*, 2010a; Jiang *et al.*, 2015b). The negative effect of H_2O might be ascribed to the competitive adsorption between H_2O and reactants or the positioning of oxygen vacancies (Gao *et al.*, 2010a). The positive effect of H_2O at 500°C was possibly due to the inhibition of NH_3 oxidation (Gao *et al.*, 2010a).

Fig. 6 presents the effect of SO_2 on the SCR activities of $Ce_{15}Ti$ and $Ce_{15}Nb_{10}Ti$. Before SO_2 was added to the feed gas, the NO conversions over $Ce_{15}Ti$ and $Ce_{15}Nb_{10}Ti$ were close to 100% at 350°C. In the presence of SO_2, the NO conversion over $Ce_{15}Ti$ gradually decreased with time to 42.1% after 11 h. As for $Ce_{15}Nb_{10}Ti$, although its NO conversion declined, 52.6% NO conversion was still obtained after 11 h. It could be seen that $Ce_{15}Nb_{10}Ti$ exhibited higher SO_2 resistance than $Ce_{15}Ti$. The deactivation by SO_2 of $Ce_{15}Ti$ and $Ce_{15}Nb_{10}Ti$ might be attributed to the generation of sulfate species, including NH_4HSO_4, $Ce(SO_4)_2$ and $Ce_2(SO_4)_3$ (Xu *et al.*, 2009; Wang *et al.*, 2012; Guo *et al.*, 2017). After SO_2 was cut off from the feed gas, a little activity was recovered over both catalysts. It meant that NH_4HSO_4 might volatilize or decompose (Xu *et al.*, 2009), thereby resulting in regaining their partial activities after the removal of SO_2. The deactivation by SO_2 of $Ce_{15}Ti$ and $Ce_{15}Nb_{10}Ti$ primarily originated from the formation of $Ce(SO_4)_2$ and $Ce_2(SO_4)_3$ with high thermal stability. They could disrupt the Ce^{4+}/Ce^{3+} redox cycle and inhibit the formation and adsorption of surface nitrate species (Xu

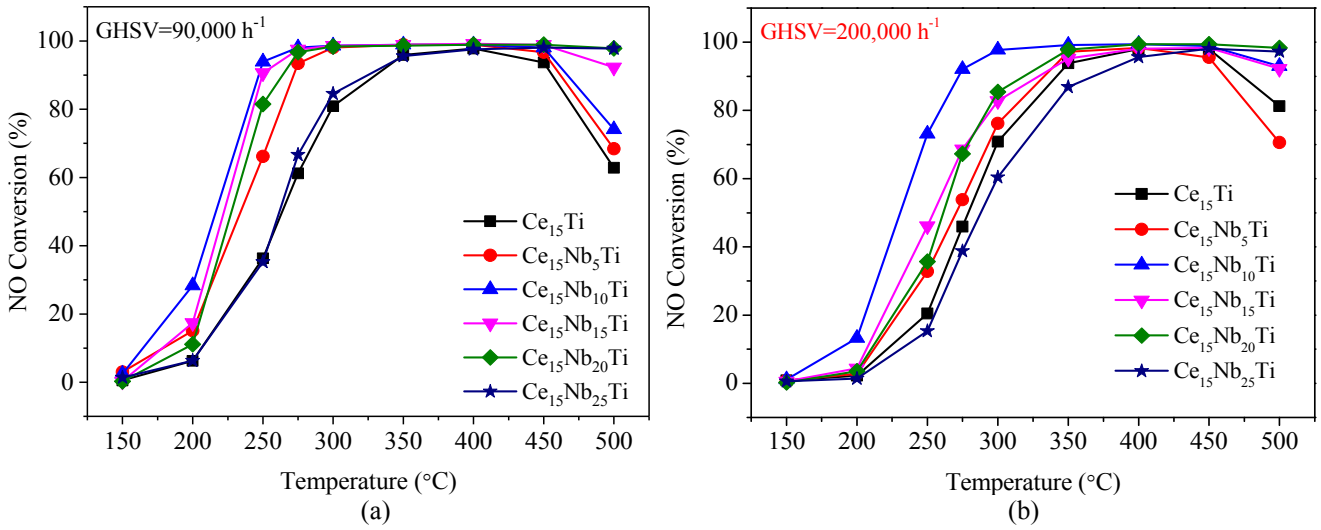

Fig. 2. NH_3-SCR activities over various catalysts with different Nb_2O_5 loadings. Reaction conditions: [NO] = [NH_3] = 1000 ppm, [O_2] = 3 vol.%, balance N_2 and GHSV = (a) 90,000 h^{-1} and (b) 200,000 h^{-1}.

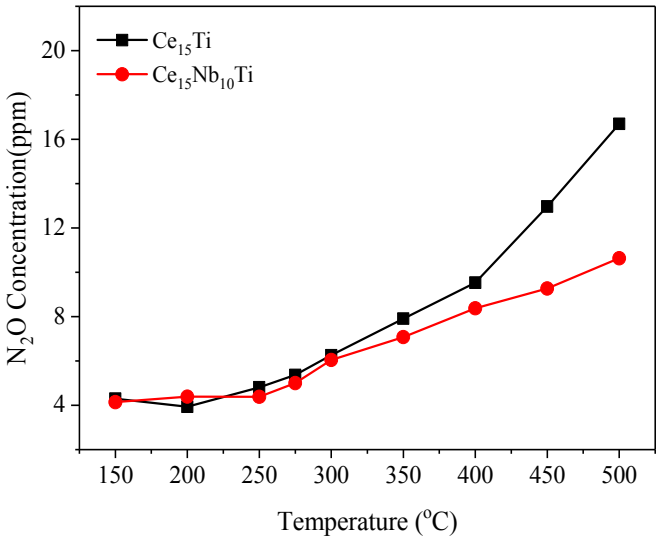

Fig. 3. N_2O conversations over $Ce_{15}Ti$ and $Ce_{15}Nb_{10}Ti$. Reaction conditions: [NO] = [NH_3] = 1000 ppm, [O_2] = 3 vol.%, GHSV = 90,000 h^{-1} and balance N_2.

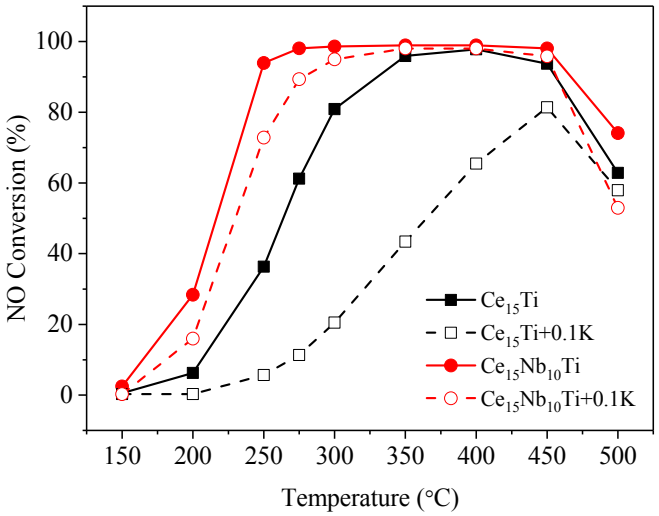

Fig. 4. Effect of K_2O on the SCR activities of $Ce_{15}Ti$ and $Ce_{15}Nb_{10}Ti$. Reaction conditions: [NO] = [NH_3] = 1000 ppm, [O_2] = 3 vol.%, GHSV=90,000 h^{-1} and balance N_2.

et al., 2009). The addition of Nb might play a certain role in hindering the formation of $Ce(SO_4)_2$ and $Ce_2(SO_4)_3$, thereby improving the resistance to SO_2 of $Ce_{15}Ti$.

Characterization of Catalysts

BET and XRD Results

The BET surface area and pore characterization of TiO_2, $Ce_{15}Ti$, $Nb_{10}Ti$ and $Ce_{15}Nb_{10}Ti$ are listed in Table 1. The surface area increased in the following sequence: $Ce_{15}Nb_{10}Ti < Nb_{10}Ti < Ce_{15}Ti < TiO_2$. The addition of Nb led to the decrease of the surface area of $Ce_{15}Ti$ and TiO_2 and the increase of their average pore diameters. However, $Ce_{15}Nb_{10}Ti$ possessed best SCR activity. It implied that the BET surface area was not a key factor to achieve excellent SCR activity for $Ce_{15}Nb_{10}Ti$.

The XRD patterns of different samples are shown in Fig. 7. Only anatase TiO_2 was detected over TiO_2 and $Nb_{10}Ti$. As for $Ce_{15}Ti$ and $Ce_{15}Nb_{10}Ti$, besides anatase TiO_2, the diffraction peaks of cubic CeO_2 were also found. No visible phase of Nb species was observed on $Nb_{10}Ti$ and $Ce_{15}Nb_{10}Ti$, which suggested that Nb species are highly dispersed on the catalyst surface. The addition of Nb seemed to induce the slight decrease in the intensity of the characteristic peaks of anatase TiO_2 and cubic CeO_2. This meant that niobium oxide could lower the crystallinity of CeO_2 and thus enhanced the dispersion of CeO_2 on the catalyst surface. In comparison with XRD and activity results, it could be speculated that cubic CeO_2 could be more susceptible to K_2O than highly dispersed CeO_2. Therefore, $Ce_{15}Nb_{10}Ti$ showed better activity than $Ce_{15}Ti$ in the presence of K_2O.

XPS Results

To identify the chemical state of surface species, $Ce_{15}Ti$ and $Ce_{15}Nb_{10}Ti$ were analyzed by XPS. The photoelectron

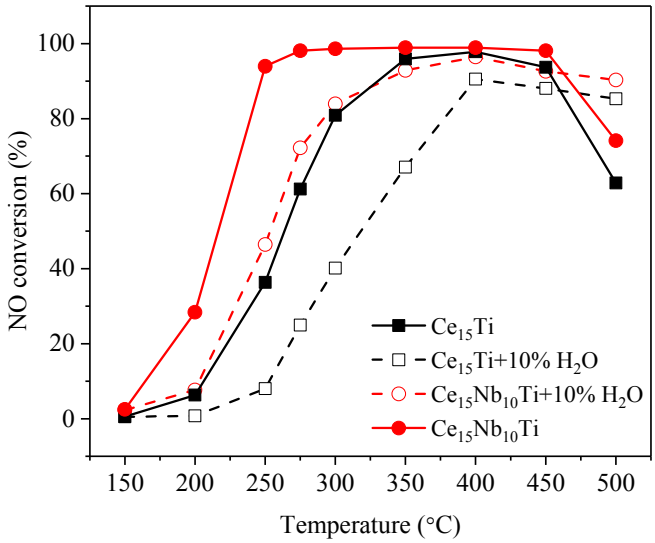

Fig. 5. Effect of H_2O on the SCR activities of $Ce_{15}Ti$ and $Ce_{15}Nb_{10}Ti$ catalysts. Reaction conditions: [NO] = [NH_3] = 1000 ppm, [O_2] = 3%, [H_2O] = 10%, GHSV = 90,000 h^{-1} and N_2 as balance.

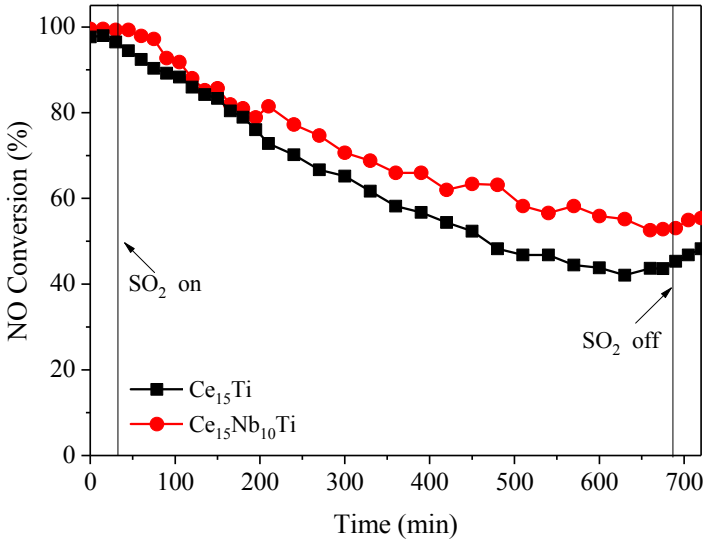

Fig. 6. Effect of SO_2 on the SCR activities of $Ce_{15}Ti$ and $Ce_{15}Nb_{10}Ti$ catalysts at 350°C. Reaction conditions: [NO] = [NH_3] = 1000 ppm, [O_2] = 3%, [SO_2] = 200 ppm, GHSV = 90,000 h^{-1} and N_2 as balance.

Table 1. Physical properties of various samples.

Samples	BET surface area (m^2 g^{-1})	Average pore diameter (nm)	Total pore volume (cm^3 g^{-1})
TiO_2	97.90	8.90	0.2437
$Ce_{15}Ti$	76.07	12.74	0.2824
$Nb_{10}Ti$	74.96	11.02	0.2400
$Ce_{15}Nb_{10}Ti$	71.76	12.74	0.2630

spectra of Ti 2p, Ce 3d and O 1s are presented in Fig. 8. As shown in Fig. 8(a), for $Ce_{15}Ti$, the binding energies of two peaks were 464.5 and 458.8 eV, respectively. This indicated that Ti existed in Ti^{4+} over $Ce_{15}Ti$ (Du *et al.*, 2012; Jiang *et al.*, 2014). After the addition of Nb, the binding energies moved to higher values and increased to 464.8 and 459.1 eV. Du *et al.* (2012) found the similar phenomena over V-Sb-Nb/TiO_2 catalyst. Referring to the handbook of XPS (Wagner *et al.*, 1979), Ti still existed in the form of Ti^{4+} after the addition of Nb. Furthermore, it could be also seen that the intensity of Ti 2p peaks of $Ce_{15}Nb_{10}Ti$ was obviously lower than those of $Ce_{15}Ti$ and $Nb_{10}Ti$. This indicated that there was the strong interaction among Ce, Nb and Ti species.

As exhibited in Fig. 8(b), the Ce 3d XPS peaks denoted as u, u″, u‴ and v, v″, v‴ could be attributed to Ce^{4+}, while

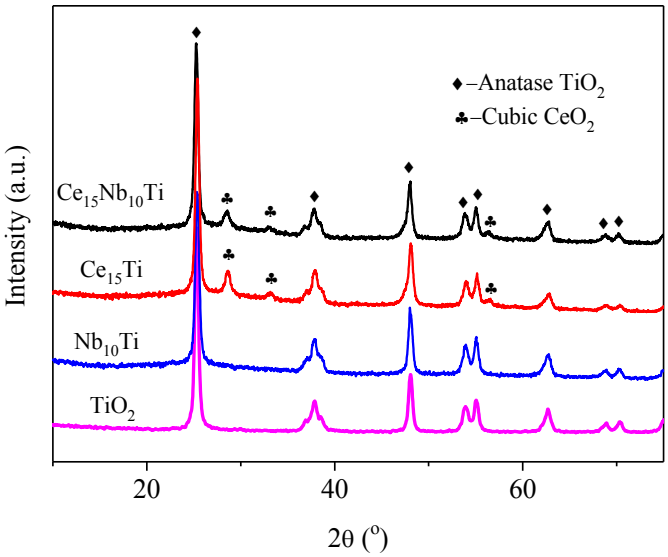

Fig. 7. XRD patterns of different catalysts.

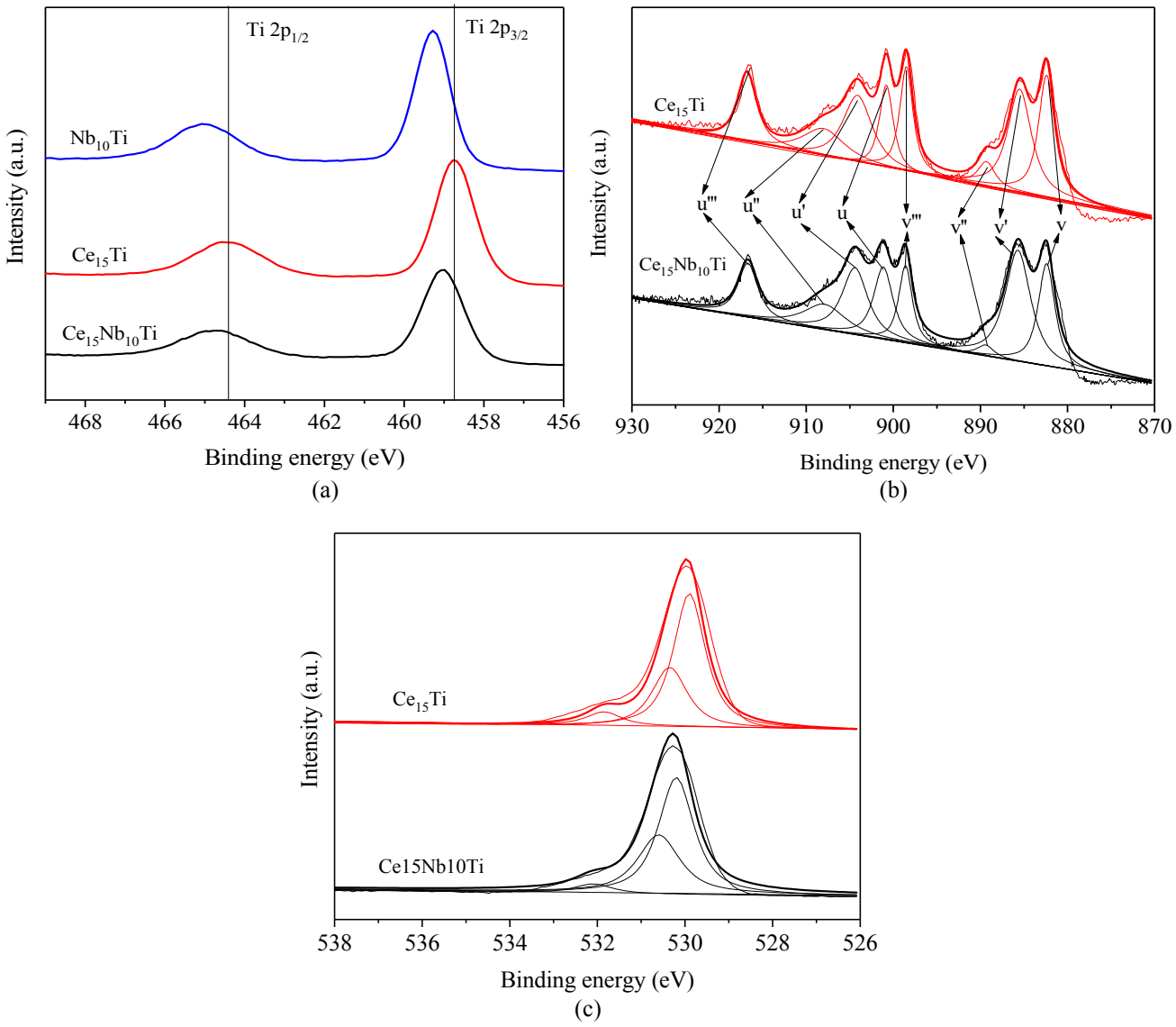

Fig. 8. XPS spectra of (a) Ti 2p, (b) Ce 3d, and (c) O 1s for $Ce_{15}Ti$ and $Ce_{15}Nb_{10}Ti$.

u′ and v′ could be assigned to Ce^{3+} (Burroughs *et al.*, 1976; Jiang *et al.*, 2015a, b). It could be seen that the intensities of Ce^{3+} characteristic peaks increased after the doping of Nb, accompanied with a decline in the intensities of Ce^{4+} characteristic peaks. Similar phenomena were also observed on Ce-Nb oxide catalyst (Qu *et al.*, 2013). The Ce^{3+} ratio of $Ce_{15}Nb_{10}Ti$ (41.3%), calculated by $Ce^{3+}/(Ce^{3+} + Ce^{4+})$, was obviously higher than of $Ce_{15}Ti$ (36.5%). The increase in the amount of Ce^{3+} resulted from the fact that the interaction between Nb and Ce species could promote the reduction of Ce^{4+} to Ce^{3+}. Higher Ce^{3+} ratio is indicative of more oxygen vacancies, which were beneficial to adsorb and activate reactant species (Liu *et al.*, 2013; Geng *et al.*, 2017; Jiang *et al.*, 2017).

The O 1s XPS spectra of $Ce_{15}Ti$ and $Ce_{15}Nb_{10}Ti$ could be fitted into three overlapping peaks (see Fig. 8(c)). They were referred to the lattice oxygen at 528.5–529.0 eV (denoted by Oβ), the chemisorbed oxygen at 528.7–529.5 eV (denoted by Oα) from oxide defects or hydroxyl-like groups, and the surface oxygen by hydroxyl species and/or adsorbed water species at 529.0–530.5 eV (denoted by Oγ) (Dupin *et al.*, 2000; Eom *et al.*, 2008; Liu *et al.*, 2017). The relative ratio of Oα calculated by Oα/(Oα + Oβ + Oγ) on $Ce_{15}Nb_{10}Ti$ (35.1%) was much higher than that on $Ce_{15}Ti$ (30.5%). It suggested that the amount of chemisorbed oxygen increased after the introduction of niobium. High Oα ratio is considered to be beneficial to the NO oxidation to NO_2 in the SCR reaction and thereafter facilitate the "fast SCR" reaction (Kang *et al.*, 2007; Wu *et al.*, 2008). These XPS results confirmed that the increase of Ce^{3+} was accompanied by the increment in oxygen vacancies and active oxygen species, which played a positive role in the SCR activity of $Ce_{15}Nb_{10}Ti$.

TEM Results

The HR-TEM micrographs of different catalysts are displayed in Fig. 9. The microscope gave a clear view on the morphology and crystal structure of $Ce_{15}Ti$ and $Ce_{15}Nb_{10}Ti$. It could be seen that the two samples stayed in the form of oval-shaped anatase crystal particles. No fringes attributed to Nb species were observed over the two samples. It meant that Nb species dispersed well on support TiO_2 for the two samples. For $Ce_{15}Ti$, there were three kinds of lattice fringes. 0.286 nm, 0.332 nm and 0.357 nm of lattice fringes matched CeO_2 (200) phase (Corrêa *et al.*, 2011), rutile (110) phase (Zhou *et al.*, 2017) and anatase (101) phase (Sutradhar *et al.*, 2014), respectively. It should be noted that rutile phase was not determined in XRD. The reason might be that rutile TiO_2 was well dispersed and existed as an amorphous or highly dispersed species in $Ce_{15}Ti$. The detected rutile phase indicated little sintering of anatase TiO_2 in $Ce_{15}Ti$. However, only 0.283 nm (matching CeO_2 (200) phase; Corrêa *et al.*, 2011) and 0.358 nm (matching anatase (101) phase; Sutradhar *et al.*, 2014) of lattice fringes could be observed on the $Ce_{15}Nb_{10}Ti$ surface. This showed that the addition of Nb could inhibit the sintering of anatase TiO_2. This was beneficial to increase the dispersion of CeO_2 on anatase TiO_2, allowing to improve the catalytic activity.

H_2-TPR Analysis

Fig. 10 illustrates the H_2-TPR profiles of $Ce_{15}Ti$ and $Ce_{15}Nb_{10}Ti$ to estimate the reducibility of two catalysts. The onset reduction temperature of the peaks of two catalysts was 315°C. There was one broad peak at 550°C on the H_2-TPR profile of $Ce_{15}Ti$ in the test temperature range, which was similar to that of CeO_2/TiO_2 catalyst (Chen *et al.*, 2012). This peak could be ascribed to the reduction of surface oxygen species of ceria (Chen *et al.*, 2012; Ma *et al.*, 2012). As for $Ce_{15}Nb10Ti$, it was obvious that a new reduction peak appeared at about 520°C. This might originate from the difference in the type and strength of the interaction among Ce, Ti and Nb species. The lower the temperature of reduction peak was, the more easily the catalyst was reduced (Ma *et al.*, 2015). In addition, it was found that the amount of H_2 consumption over $Ce_{15}Ti$ was less than that over $Ce_{15}Nb_{10}Ti$ (1:2.27). It implied more surface oxygen species on $Ce_{15}Nb_{10}Ti$, which was in accordance with the XPS results. These could the reason why the Ce_xNb_yTi catalysts exhibited excellent activity than $Ce_{15}Ti$.

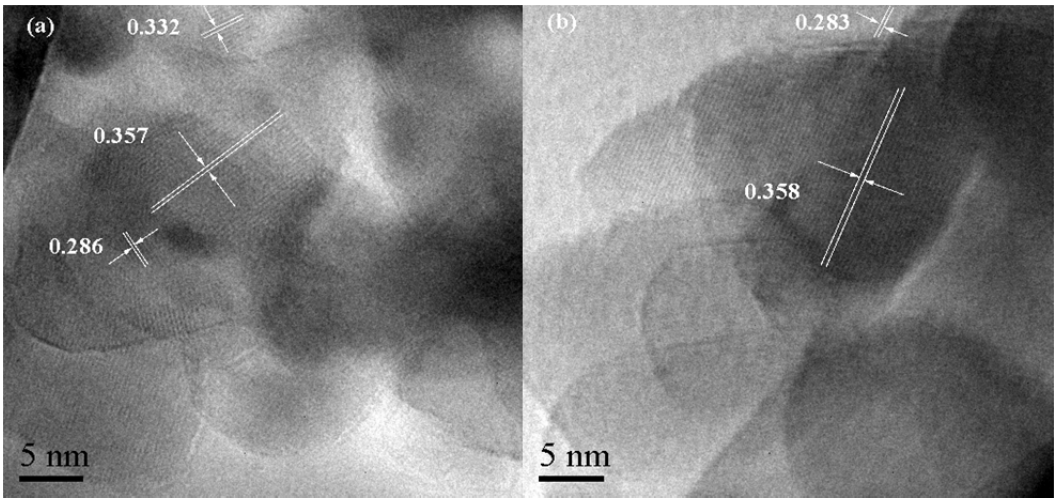

Fig. 9. TEM images of (a) $Ce_{15}Ti$ and (b) $Ce_{15}Nb_{10}Ti$.

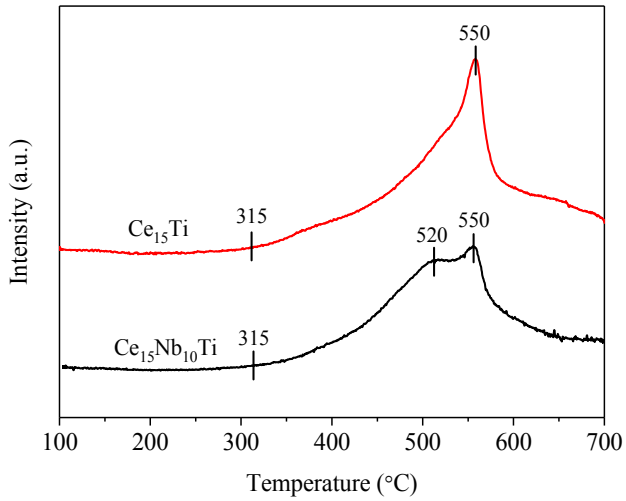

Fig. 10. H_2-TPR profiles of $Ce_{15}Ti$ and $Ce_{15}Nb_{10}Ti$.

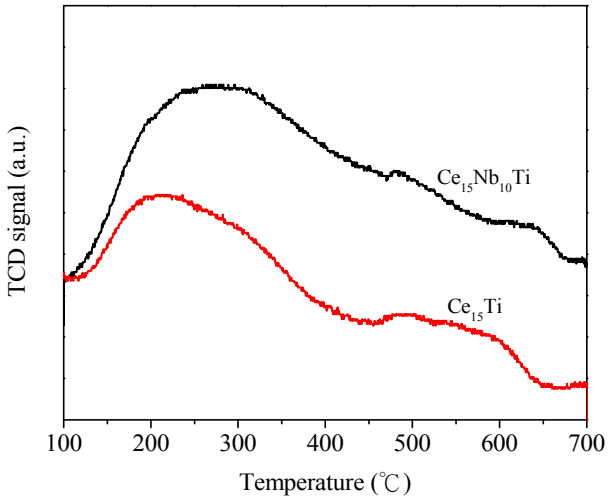

Fig. 11. NH_3-TPD profiles of $Ce_{15}Ti$ and $Ce_{15}Nb_{10}Ti$.

NH_3-TPD Analysis

NH_3-TPD was performed to characterize the surface acidity of the catalysts and the results are seen in Fig. 11. Both $Ce_{15}Ti$ and $Ce_{15}Nb_{10}Ti$ possessed two desorption peaks in the temperature range of about 100–400°C and 450–675°C. The areas of both NH_3 desorption peaks over $Ce_{15}Nb_{10}Ti$ were obviously larger than those over $Ce_{15}Ti$, especially that of low-temperature desorption peak. The low-temperature and high-temperature peaks belonged to the weakly and strongly bonded NH_3, respectively (Cai *et al.*, 2014). It was reported that the NH_3 bound to Brønsted acid sites are less thermally stable than the coordinated NH_3 molecules bound to Lewis acid sites and could desorb at lower temperatures (Zhao *et al.*, 2016). It meant that the introduction of Nb could increase the amount of Brønsted and Lewis acid sites. Furthermore, the amount of Brønsted acid sites increased more dramatically. The increase in the Brønsted and Lewis acidity helped to enhance the adsorption capacity of NH_3 species on the catalyst, thereby favoring the SCR reaction.

CONCLUSIONS

$Ce_{15}Nb_{10}Ti$ possessed excellent catalytic activity even at a high GHSV of 200,000 h^{-1} in the temperature range of 275–450°C. It also exhibited a higher resistance than $Ce_{15}Ti$ to K_2O, H_2O and SO_2. The Ce-Ti oxides with and without Nb were characterized using BET, XRD, XPS, TEM, H_2-TPR and NH_3-TPD. The results indicate that the introduction of Nb could improve the dispersion of Ce species on the TiO_2 support. Compared with cubic CeO_2, highly dispersed CeO_2 was likely to have a higher resistance to K. XPS results reveal that the interaction between Nb and Ce species could promote the transformation of Ce^{4+} into Ce^{3+}. As a result, the amount of Ce^{3+} increased, accompanied by an increase in oxygen vacancies and active oxygen species, which play a positive role in the SCR reaction over Ce-Ti oxide. H_2-TPR results demonstrate the enhanced reducibility of the Ce-Ti oxide after being doped with Nb. NH_3-TPD results reveal the increase in surface acidity, especially due to the increase in the number of Brønsted acid sites, leads to a marked increase in the amount of NH_3 absorbed on the surface of $Ce_{15}Nb_{10}Ti$. Based on these results, the excellent SCR performance of $Ce_{15}Nb_{10}Ti$ could be attributed to the high dispersion of CeO_2 and Nb_2O_5 on the TiO_2 surface, the increased amount of Ce^{3+} and surface chemisorbed oxygen, the improvement in surface acidity and reducibility, and the synergetic interaction among Ce, Nb and Ti species.

ACKNOWLEDGMENTS

This work was supported by the National Natural Science Foundation of China (No. 51506226), Natural Science Foundation of Shandong Province (No. ZR2015EM010), "the Fundamental Research Funds for the Central Universities" (No. 15CX05005A) and the scholarship from China Scholarship Council, China (CSC) (No. 201706455013).

REFERENCES

Burroughs, P., Hamnett, A., Orchard, A.F. and Thornton, G. (1976). Satellite structure in the X-ray photoelectron spectra of some binary and mixed oxides of lanthanum and cerium. *J. Chem. Soc. Dalton Trans.* 17: 1686–1698.

Busca, G., Lietti, L., Ramis, G. and Berti, F. (1998). Chemical and mechanistic aspects of the selective catalytic reduction of NO_x by ammonia over oxide catalysts: A review. *Appl. Catal. B* 18: 1–36.

Cai, S., Zhang, D., Zhang, L., Huang, L. and Li, H. (2014). Comparative study of 3D ordered macroporous $Ce_{0.75}Zr_{0.2}M_{0.05}O_{2-\delta}$ (M=Fe, Cu, Mn, Co) for selective catalytic reduction of NO with NH_3. *Catal. Sci. Technol.* 4: 93–101.

Casapu, M., Kröcher, O., Mehring, M., Nachtegaal, M., Borca, C., Harfouche, M. and Grolimund, D. (2010). Characterization of Nb-containing MnO_x-CeO_2 catalyst for low-temperature selective catalytic reduction of NO with NH_3. *J. Phys. Chem. C* 114: 9791–9801.

Chen, L., Li, J., Ge, M. and Zhu, R. (2010). Enhanced

activity of tungsten modified CeO_2/TiO_2 for selective catalytic reduction of NO_x with ammonia. *Catal. Today* 153: 77–83.

Chen, L., Weng, D., Si, Z. and Wu, X. (2012). Synergistic effect between ceria and tungsten oxide on WO_3-CeO_2-TiO_2 catalysts for NH_3-SCR reaction. *Prog. Nat. Sci. Mater. Int.* 22: 265–272.

Chen, L., Si, Z., Wu, X., Weng, D. and Wu, Z. (2015). Effect of water vapor on NH_3–NO/NO_2 SCR performance of fresh and aged MnO_x-NbO_x-CeO_2 catalysts. *J. Environ. Sci.* 31: 240–247.

Corrêa, D.N., de Souza e Silva, J.M., Santos, E.B., Sigoli, F.A., Souza Filho, A.G. and Mazali, I.O. (2011). TiO_2- and CeO_2-based biphasic core–shell nanoparticles with tunable core sizes and shell thicknesses. *J. Phys. Chem. C* 115: 10380–10387.

Du, X., Gao, X., Fu, Y., Gao, F., Luo, Z. and Cen. K. (2012). The co-effect of Sb and Nb on the SCR performance of the V_2O_5/TiO_2 catalyst research article. *J. Colloid Interface Sci.* 368: 406–412.

Du, X., Xue, J., Wang, X., Chen, Y., Ran, J. and Zhang, L. (2018). Oxidation of sulfur dioxide over V_2O_5/TiO_2 catalyst with low vanadium loading: A theoretical study. *J. Phys. Chem. C* 122: 4517–4523.

Dunn, J.P., Koppula, P.R., Stenger, H.G. and Wachs I.E. (1998). Oxidation of sulfur dioxide to sulfur trioxide over supported vanadia catalysts. *Appl. Catal. B* 19: 103–117.

Dupin, J.C., Gonbeau, D., Vinatier, P. and Levasseur, A. (2000). Systematic XPS studies of metal oxides, hydroxides and peroxides. *Phys. Chem. Chem. Phys.* 2: 1319–1324.

Eom, Y., Jeon, S.H., Ngo, T.A., Kim, J. and Lee, T.G. (2008). Heterogeneous mercury reaction on a selective catalytic reduction (SCR) catalyst. *Catal. Lett.* 121: 219–225.

Fu, M., Li, C., Lu, P., Qu, L., Zhang, M., Zhou, Y., Yu, M. and Fang, Y. (2014). A review on selective catalytic reduction of NO_x by supported catalysts at 100-300°C– catalysts, mechanism, kinetics. *Catal. Sci. Technol.* 4: 14–25.

Gao, X., Du, X., Cui, L., Fu, Y., Luo, Z. and Cen, K. (2010a). A Ce–Cu–Ti oxide catalyst for the selective catalytic reduction of NO with NH_3. *Catal. Commun*. 12: 255–258.

Gao, X., Jiang, Y., Zhong, Y., Luo, Z. and Cen, K. (2010b). The activity and characterization of CeO_2-TiO_2 catalysts prepared by the sol-gel method for selective catalytic reduction of NO with NH_3. *J. Hazard. Mater.* 174: 734–739.

Geng, Y., Chen, X., Yang, S., Liu, F. and Shan, W. (2017). Promotional effects of Ti on a CeO_2-MoO_3 catalyst for the selective catalytic reduction of NO_x with NH_3. *Appl. Mater. Interfaces* 9: 16951–16958.

Guo, R., Zhou, Y., Pan, W., Hong, J., Zheng, W., Jin, Q., Ding, C. and Guo, S. (2013). Effect of preparation methods on the performance of $CeO_2/Al2O_3$ catalysts for selective catalytic reduction of NO with NH_3. *J. Ind. Eng. Chem.* 19: 2022–2025.

Guo, R., Sun, P., Pan, W., Li, M., Liu, S., Sun X., Liu, S. and Liu, J. (2017). A Highly effective $MnNdO_x$ catalyst for the selective catalytic reduction of NO_x with NH_3. *Ind. Eng. Chem. Res*. 56: 12566–12577.

Jiang, Y., Gao, X., Zhang, Y., Wu, W., Song, H., Luo, Z. and Cen, K. (2014). Effects of $PbCl_2$ on selective catalytic reduction of NO with NH_3 over vanadia-based catalysts. *J. Hazard. Mater.* 274: 270–278.

Jiang, Y., Xing, Z., Wang, X., Huang, S., Liu, Q. and Yang, J. (2015a). MoO_3 modified CeO_2/TiO_2 catalyst prepared by a single step sol-gel method for selective catalytic reduction of NO with NH_3. *J. Ind. Eng. Chem*. 29: 43–47.

Jiang, Y., Xing, Z., Wang, X., Huang, S., Wang, X. and Liu, Q. (2015b). Activity and characterization of a Ce-W-Ti oxide catalyst prepared by a single step sol-gel method for selective catalytic reduction of NO with NH_3. *Fuel* 151: 124–129.

Jiang, Y., Wang, X., Xing, Z., Bao, C. and Liang, G. (2017). Preparation and characterization of CeO_2-MoO_3/TiO_2 catalysts for selective catalytic reduction of NO with NH_3. *Aerosol Air Qual. Res.* 17: 2726–2734.

Kang, M., Park, E.D., Kim, J.M. and Yie, J.E. (2007). Manganese oxide catalysts for NO_x reduction with NH_3 at low temperatures. *Appl. Catal. A* 327: 261–269.

Li, P., Xin, Y., Li, Q., Wang, Z., Zhang, Z. and Zheng, L. (2012). Ce-Ti amorphous oxides for selective catalytic reduction of NO with NH_3: Confirmation of Ce-O-Ti active sites. *Environ. Sci. Technol.* 46: 9600–9605.

Li, Q., Liu, H., Chen, T., Chen, D., Zhang, C., Xu, B., Zhu, C. and Jiang, Y. (2017). Characterization and SCR performance of nano-structured iron-manganese oxides: Effect of annealing temperature. *Aerosol Air Qual. Res.* 17: 2328–2337.

Lian, Z., Liu, F., He, H., Shi, X., Mo, J. and Wu, Z. (2014). Manganese-niobium mixed oxide catalyst for the selective catalytic reduction of NO_x with NH_3 at low temperatures. *Chem. Eng. J.* 250: 390–398.

Lian, Z., Liu, F., He, H. and Liu, K. (2015). Nb-doped VO_x/CeO_2 catalyst for NH_3-SCR of NO_x at low temperatures. *RSC Adv.* 5: 37675–37681.

Liu, C., Chen, L., Chang, H., Ma, L., Peng, Y., Arandiyan, H. and Li, J. (2013). Characterization of CeO_2-WO_3 catalysts prepared by different methods for selective catalytic reduction of NO_x with NH_3. *Catal. Commun.* 40: 145–148.

Liu, H., Zhang, Z., Li, Q., Chen, T., Zhang, C., Chen, D., Zhu, C. and Jiang, Y. (2017). Novel method for preparing controllable nanoporous α-Fe_2O_3 and its reactivity to SCR De-NO_x. *Aerosol Air Qual. Res.* 17: 1898–1908.

Liu, Z., Zhang, S., Li, J. and Ma, L. (2014). Promoting effect of MoO_3 on the NO_x reduction by NH_3 over CeO_2/TiO_2 catalyst studied with in situ DRIFTS. *Appl. Catal. B* 144: 90–95.

Ma, Z., Weng, D., Wu, X. and Si, Z. (2012). Effects of WO_x modification on the activity, adsorption and redox properties of CeO_2 catalyst for NO_x reduction with ammonia. *J. Environ. Sci.* 24: 1305–1316.

Ma, Z., Wu, X., Si, Z., Weng, D., Ma, J. and Xu, T. (2015).

Impacts of niobia loading on active sites and surface acidity in NbO_x/CeO_2–ZrO_2 NH_3-SCR catalysts. *Appl. Catal. B* 179: 380–394.

Nakajima, F. and Hamada, I. (1996). The state-of -the-art technology of NO_x control. *Catal. Today* 29: 109–115.

Qu, R., Gao, X., Cen, K. and Li, J. (2013). Relationship between structure and performance of a novel cerium-niobium binary oxide catalyst for selective catalytic reductionof NO with NH_3. *Appl. Catal. B* 142–143: 290–297.

Shan, W., Liu, F., Hong, H., Shi, X. and Zhang, C. (2011). The remarkable improvement of a Ce-Ti based catalyst for NO_x abatement, prepared by a homogeneous precipitation method. *ChemCatChem* 3: 1286–1289.

Shan, W., Liu, F., He, H., Shi, X. and Zhang, C. (2012). A superior Ce-W-Ti mixed oxide catalyst for the selective catalytic reduction of NO_x with NH_3. *Appl. Catal. B* 115–116: 100–106.

Shen, Y., Zhu, S., Qiu, T. and Shen, S. (2009). A novel catalyst of $CeO_2/Al2O_3$ for selective catalytic reduction of NO by NH_3. *Catal. Commun.* 11: 20–23.

Sutradhar, N., Biswas, A.K., Pahari, S.K., Ganguly, B. and Panda, A.B. (2014). Fluoride free synthesis of anatase TiO_2 nanocrystals with exposed active {001} facets. *Chem. Commun.* 50: 11529–11532.

Vikulov, K.A., Andreini, A., Poels, E.K. and Bliek, A. (1994). Selective catalytic reduction of NO with NH_3 over Nb_2O_5-promoted V_2O_5/TiO_2 catalysts. *Catal. Lett.* 25: 49–54.

Wagner, C.D., Riggs, W.M., Davis, L.E., Moulder, J.F. and Mullenberg, G.E. (1979). *Handbook of X-ray photoelectron spectroscopy*, Perkin-Elmer Corporation, Minnesota.

Wang, X., Du, X., Zhang, L., Chen, Y., Yang, G. and Ran, J. (2018). Promotion of NH_4HSO_4 decomposition in NO/NO_2 contained atmosphere at low temperature over V_2O_5-WO_3/TiO_2 catalyst for NO reduction. *Appl. Catal. A* 559: 112–121.

Wu, Z., Jin, R., Liu, Y. and Wang, H. (2008). Ceria modified MnO_x/TiO_2 as a superior catalyst for NO reduction with NH_3 at low-temperature. *Catal. Commun.* 9: 2217–2210.

Xu, W., Yu, Y., Zhang, C. and Hong, H. (2008). Selective catalytic reduction of NO by NH_3 over a Ce/TiO_2 catalyst. *Catal. Commun.* 9: 1453–1457.

Xu, W., He, H. and Yu, Y. (2009). Deactivation of a Ce/TiO_2 catalyst by SO_2 in the selective catalytic reduction of NO by NH_3. *J. Phys. Chem.* 113: 4426–4432.

Yates, M., Martín, J.A., Martín-Luengo, M.Á., Suárez, S. and Blanco, J. (1996). N_2O formation in the ammonia oxidation and in the SCR process with V_2O_5-WO_3 catalysts. *Catal. Today* 107–108: 120–125.

Yu, X., Cao, F., Zhu, X., Gao, X., Luo, Z. and Cen, K. (2017). Selective catalytic reduction of NO over Cu–Mn/OMC catalysts: Effect of preparation method. *Aerosol Air Qual. Res.* 17: 302–313.

Zhao, K., Han, W., Lu, G., Lu, J., Tang, Z. and Zhen, X. (2016). Promotion of redox and stability features of doped Ce-W-Ti for NH_3-SCR reaction over a wide temperature range. *Appl. Surf. Sci.* 379: 316–322.

Zhou, T., Lv, W., Li, J., Zhou, G., Zhao, Y., Fan, S., Liu, B., Li, B., Kang, F. and Yang, Q. (2017). Twinborn TiO_2-TiN heterostructures enabling smooth trapping-diffusion-conversion of polysulfides towards ultralong life lithium–sulfur batteries. *Energy Environ. Sci.* 10: 1694–1703.

Received for review, March 18, 2018
Revised, May 25, 2018
Accepted, June 26, 2018